Progress In Electromagnetics Research C, Vol. 118, 159–175, 2022

Design and Analysis of a Versatile Undesired Radiation Suppression Scheme in the Domain of Collaborative Beamforming

Robert Macharia[1, *], Kibet Langat[2], and Peter Kihato[2]

Abstract—A typical outcome of Collaborative Beamforming (CB) in Wireless Sensor Networks (WSNs) is the presence of relatively high radiation in undesired directions, an aspect attributed to the usual random arrangement of collaborating sensor nodes. High radiation in undesired directions and prominent sidelobes are bound to result in interference in adjacent co-channel networks. Research towards suppression of radiation in undesired directions in CB is active with a number of proposals already in place. Most of the proposals are in the domain/perspective of 2-dimension WSN configuration with a focus on suppressing the highest-leveled (peak) sidelobe only. Commonly, peak sidelobe suppression is achieved through nodes' transmission amplitude perturbation after a conventional phase steering based beamsteering procedure. In this paper, concurrent amplitude and phase perturbation at collaborating nodes has been utilized towards achieving concurrent beamsteering and suppression of radiation in an elaborate set of undesired directions. A variant of the Particle Swarm Optimization (PSO) algorithm has been applied in the node transmit amplitude and phase perturbation process. Selection of radiation suppression directions is done uniformly from the set of all possible undesired radiation directions. A WSN featuring planar node arrangement with the sink at an elevated plane has been used as the analysis platform. The proposed scheme outperforms the peak sidelobe suppression approach in terms of observed radiation in undesired directions and average sidelobe levels. It has also been established that increasing the number of collaborating nodes and/or the number of selected undesired radiation directions in the proposed CB scheme leads to undesired radiation performance improvement although at an exponentially decaying rate.

1. INTRODUCTION

A typical outcome of Collaborative Beamforming (CB) is relatively high radiation in undesired directions [1]. The usual random arrangement of sensor nodes in Wireless Sensor Networks (WSNs) is bound to result in high-leveled and asymmetrical sidelobes/high radiation in undesired directions upon CB [2]. This effect is more pronounced if the number of collaborating nodes in a CB process is small. High radiation in undesired directions/high-leveled sidelobes is bound to result in interference in adjacent co-channel networks. This has a negative effect on communication capacity. High sidelobe levels also imply wasted radiation energy, and energy is usually a limited resource in WSN sensor nodes.

Research towards peak sidelobe suppression in CB is active. A case in point is the work presented in [3, 4] wherein a scheme towards sidelobe suppression through node location perturbation is presented. Although substantially good results are obtained, the proposed methods rely significantly on node mobility. The proposed scheme is inapplicable to WSNs featuring nodes without a mobility mechanism. The proposed approach also implies energy usage to invoke/actualize node movement (energy is a limited resource in WSN nodes) in situations featuring mobility capable nodes.

Received 11 October 2021, Accepted 28 January 2022, Scheduled 21 February 2022

* Corresponding author: Robert Macharia (robertisaacm@gmail.com).

[1]?, Pan African University Institute for Basic Sciences, Technology and Innovation, Kenya. [2] Jomo Kenyatta University of Agriculture and Technology, Kenya.

Researchers in [5–9] advocate peak sidelobe suppression through node selection mechanisms. However, node selection is only feasible in high density WSNs. Also, there is increased possibility of overuse of selected nodes particularly if the beamsteering direction (direction of the data sink) is static.

An energy efficient CB approach towards peak sidelobe suppression is proposed in [10]. Fairly appreciable results are obtained. However, a generalized sidelobe suppression mechanism promises better performancethan the proposed peak sidelobe suppression scheme.

In [11], a study towards minimizing the peak sidelobe level of an antenna array beam pattern alongside null steering is presented. The work utilizes Atom Search Optimization (ASO) algorithm to generate optimal amplitude and phase weights. Despite appreciable results, undesired radiation suppression is focused on the peak sidelobe and specific nulling points only.

In [12], an adaptive beamforming procedure featuring sidelobe suppression through placement of "extra" radiation nulls is presented. Nulling directions are iteratively placed in the directions of the highest sidelobes. Nulling in the identified directions is accomplished through conventional beamforming mechanisms. The approach is noted to yield low sidelobe levels. However, radiation suppression in all undesired directions is bound to yield better outcomes.

Other studies in the domain of sidelobe cancellation can be found in [13–16].

In general, observations made in the reviewed literature are as per the listing below.

(i) The proposals are in the domain/perspective of 2-dimension WSN configuration wherein the data sink (access point) lies in the sensor nodes' plane.

(ii) Focus is on suppressing the peak sidelobe only.

(iii) In a large number of cases, sidelobe suppression is through nodes' transmission amplitude perturbation after a conventional phase steering based beamsteering procedure.

In this paper, a novel mechanism towards generalized reduction of radiation in undesired directions using a variant of the Particle Swarm Optimization (PSO) algorithm is brought to the fore. This paper is structured as follows. Section 2 presents the utilized collaborative beamforming model. In Section 3, the formulation of the proposed generalized radiation suppression scheme is presented. Section 4 presents an analysis of the obtained results. The paper summary/conclusion is given in Section 5.

2. COLLABORATIVE BEAMFORMING MODEL

The adopted WSN model features a planar node layout with the sink at an elevated plane. This approach is sufficient for modelling scenarios in which sensor nodes are deployed on planar or nearly-planar surfaces. The general array factor corresponding to CB through the adopted WSN model is given in Section 2.1. The exact sensor node placement utilized in this paper is given in Section 2.2.

2.1. Collaborative Beamforming Array Factor

Figure 1 illustrates a typical WSN model featuring 2-dimension random arrangement of sensor nodes. The sink is placed at some location (A_0, ϕ_0, θ_0).

With reference to Fig. 1, the distance between node t and the sink is as per Eq. (1).

$$d_t|_{(A_0,\phi_0,\theta_0)} = \sqrt{A_0^2 + r_t^2 - 2r_t A_0 \sin\theta_0 \cos(\phi_0 - \psi_t)} \tag{1}$$

where r_t is the distance from the cluster head (at the origin) to node t, and ψ_t is the azimuthal displacement of node t as per Fig. 1.

The distance between node t and some general position (A, ϕ, θ) is as per Eq. (2).

$$d_t|_{(A,\phi,\theta)} = \sqrt{A^2 + r_t^2 - 2r_t A \sin\theta \cos(\phi - \psi_t)} \tag{2}$$

$A \gg r_t$ in the far-field radiation region; an approximate value for d_t in the far field region is as per Eq. (3).

$$d_t|_{(A,\phi,\theta)} \approx A - r_t \sin\theta \cos(\phi - \psi_t) \tag{3}$$

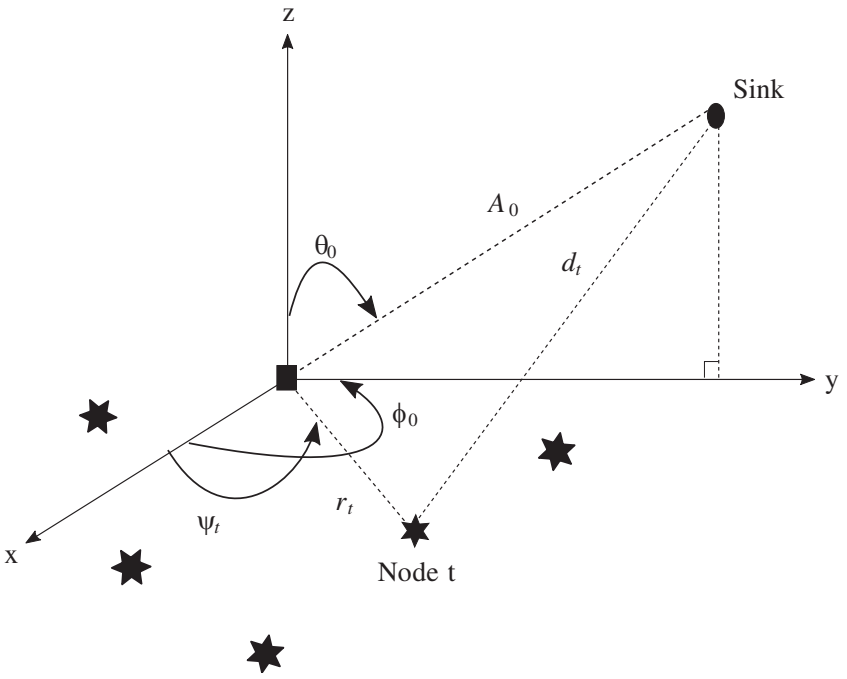

Figure 1. Wireless sensor network model with the sink at an elevated location relative to the nodes' plane. CB cluster head-*rectangular shape*; Sensor nodes-*star shape*.

The array factor for a total of T collaborating nodes, each transmitting at an amplitude equivalent to $1/T$, is as per Eq. (4).

$$AF_{\phi,\theta} = \frac{1}{T}\sum_{t=1}^{T} e^{j\Psi_t} e^{j\frac{2\pi}{\lambda}d_t(\phi,\theta)} \tag{4}$$

where:

- AF is the array factor.
- T is the total number of collaborating nodes.
- Ψ_t is the initial phase for node $t \in 1, 2, 3 \ldots T$.
- $1/T$ is the node transmit amplitude.

Using Eq. (3), the array factor as per Eq. (4) can be approximated to Eq. (5).

$$AF_{\phi,\theta} \approx \frac{1}{T}\sum_{t=1}^{T} e^{j\Psi_t} e^{j\frac{2\pi}{\lambda}[A - r_t \sin\theta\cos(\phi-\psi_t)]} \tag{5}$$

Equation (6) below is an expanded form of Eq. (5).

$$AF_{\phi,\theta} \approx \frac{1}{T}\sum_{t=1}^{T} e^{j\Psi_t} e^{j\frac{2\pi}{\lambda}A} e^{j\frac{2\pi}{\lambda}[-r_t \sin\theta\cos(\phi-\psi_t)]} \tag{6}$$

The term $e^{j\frac{2\pi}{\lambda}A}$ in Eq. (6) is a constant phase offset, which bears no impact on the directional properties of $AF_{\phi,\theta}$. As such, the term has been dropped in subsequent derivations. The node transmitting phase (Ψ_t) and amplitude ($1/T$) can be varied to alter the array factor to a desired form, for instance to steer the main beam of the overall radiation towards the sink's direction. The terms $1/T$ and $e^{j\Psi_t}$ can be combined to form a single complex node transmitting weight (w_t) yielding Eq. (7).

$$AF_{\phi,\theta} \approx \sum_{t=1}^{T} w_t e^{j\frac{2\pi}{\lambda}[-r_t \sin\theta\cos(\phi-\psi_t)]} \tag{7}$$

Upon normalizing r_t with respect to signal wavelength ($\tilde{r}_t = r_t/\lambda$), Eq. (7) can be expressed as per Eq. (8). Wavelength normalization allows for CB problem conceptualization independent of wavelength.

$$AF_{\phi,\theta} \approx \sum_{t=1}^{T} w_t e^{j2\pi[-\tilde{r}_t \sin\theta \cos(\phi-\psi_t)]} \tag{8}$$

Assuming isotropic radiators at the sensor nodes, to yield a desired radiation pattern, the array factor as per Eq. (8) can be directly manipulated by optimally varying the node transmission complex weights (w_t) (*the CB action*).

2.2. WSN Node Layout

A set of 20 nodes is configured in a planar manner as per Fig. 2. The nodes are randomly distributed over a coverage area of unit radius (the placement is wavelength-normalized). A wavelength of 0.125 m is utilized assuming an operation frequency of 2.4 GHz.

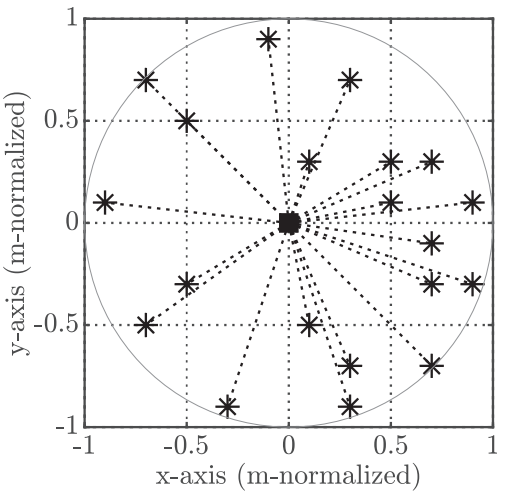

Figure 2. Node layout: A random and planar configuration over an area of unit radius (the placement is wavelength-normalized).

The nodes are assumed to lie on the 0 degrees elevation plane on a right-handed cartesian coordinate system. The data sink (access point) direction from the perspective of the right-handed cartesian coordinate system origin is *100 degrees azimuth, 55 degrees elevation.*

3. FORMULATION OF A CONCURRENT BEAMSTEERING AND UNDESIRED RADIATION SUPPRESSION SCHEME

The chief aim of the proposed scheme is to concurrently ensure accurate beamsteering and minimal radiation in all undesired directions. In practice, collaborating nodes' weight evaluations are done at the CB cluster head. The cluster head ought to share the optimal weights with the collaborating nodes. It is imperative to note that a source node can act as the cluster head to ensure general fairness in energy consumption among nodes.

Let:

- (ϕ_0, θ_0) be the direction of the intended sink (desired radiation direction) with reference to the cluster head. The cluster head is assumed to lie at the origin of a right-handed cartesian coordinate system.
- (ϕ_u, θ_u) be a substantial subset of all undesired radiation directions.
- (ϕ_{SL}, θ_{SL}) be the set of sidelobes' directions corresponding to the beamformed radiation.

The objectives to be optimized are as per Equations (9), (10) and (11).

Beamsteering is accomplished through optimizing Eq. (9).

$$\text{maximize} \qquad |AF_{\phi_0,\theta_0}(\mathbf{w})|^2 \tag{9}$$

where $\mathbf{w}$ is the beamforming weights vector.

Suppression of radiation in undesired directions is accomplished through optimizing Eq. (10) where C_u is the total sum of selected undesired radiation directions.

$$\text{minimize} \qquad \frac{\sum_u |AF_{\phi_u,\theta_u}(\mathbf{w})|^2}{C_u} \tag{10}$$

The undesired radiation directions are uniformly selected from the set of all possible radiation directions less the half power main beam region of the desired radiation direction as per Fig. 3.

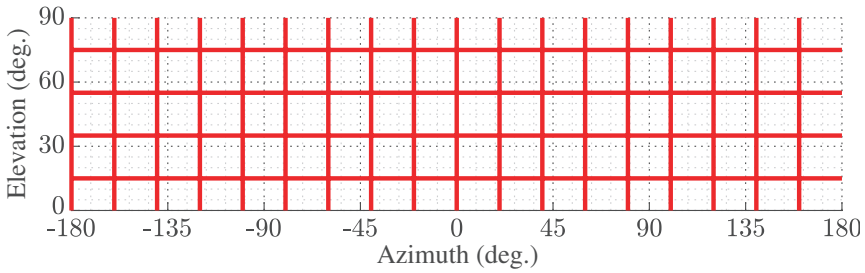

Figure 3. A representation of the selected undesired radiation directions (azimuth and elevation) taken from three dimensional space. This is as per the grid intersection points (18 by 4 points = 72 directions).

The undesired radiation selection points given in Fig. 4 are utilized in a comparative analysis process in Section 5.3.

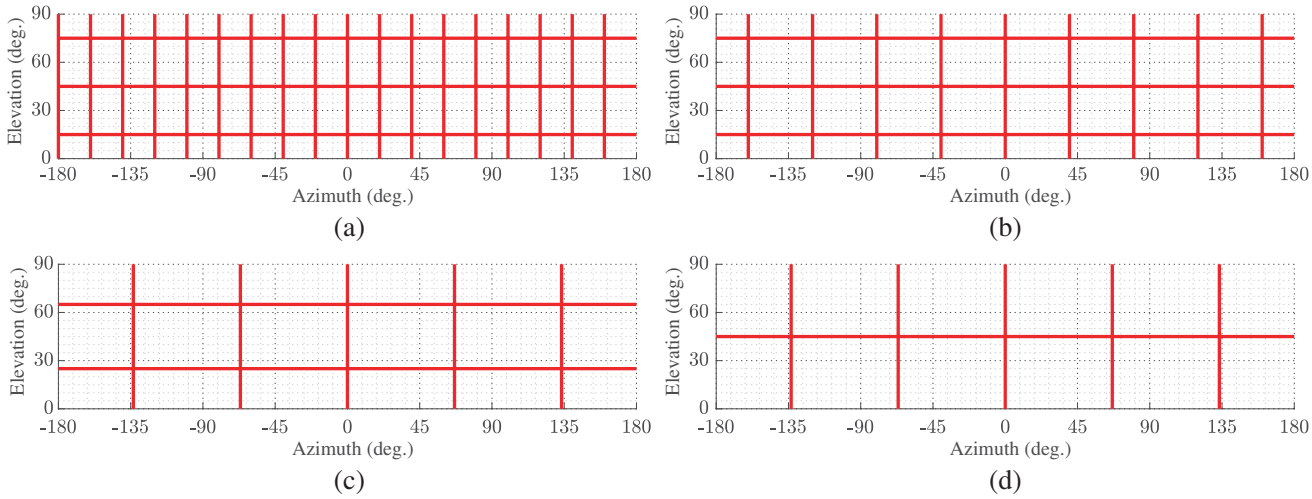

Figure 4. A representation of the selected undesired radiation directions (azimuth and elevation) taken from three dimensional space. This is as per the grid intersection points: 54, 27, 10 and 5 points/directions. (a) 18 by 3 = 54 directions. (b) 9 by 3 = 27 directions. (c) 5 by 2 = 10 directions. (d) 5 by 1 = 5 directions.

Suppression of sidelobes is accomplished through optimizing Eq. (11) where C_{SL} is the total sum of sidelobes corresponding to the beamformed radiation.

$$\text{minimize} \qquad \frac{\sum_{SL} |AF_{\phi_{SL},\theta_{SL}}(\mathbf{w})|^2}{C_{SL}} \tag{11}$$

The overall objective function to be optimized up to 20 algorithm iterations (a third the count of maximum iterations) is a combination of the objectives given in Equations (9) and (10) as per Eq. (12). In the optimization problem at hand, a maximum of 60 algorithm iterations are used. In order to effectively balance beamsteering and suppression of radiation in undesired directions, weighting values (q_x) have been utilized. The weighting values (q_x) have been carefully selected to yield the best possible outcome. In particular, the values ($q_1 = 0.7$) and ($q_2 = 0.3$) have been used.

$$\text{minimize} \qquad f(\mathbf{w}) = -q_1 |AF_{\phi_0,\theta_0}(\mathbf{w})|^2 + q_2 \frac{\sum_u |AF_{\phi_u,\theta_u}(\mathbf{w})|^2}{C_u} \tag{12}$$

The high value assigned to q_1 in comparison to that assigned to q_2 gives beamsteering higher preference in the multi-objective optimization problem. Negation of the first portion ($q_1 |AF_{\phi_0,\theta_0}(\mathbf{w})|^2$) of the multi-objective optimization function allows for the treatment of the portion as a minimization problem. This allows seamless combination of the two objectives under consideration into a single optimization (minimization) function.

The overall objective function to be optimized after 20 algorithm iterations is a weighted (g_x) combination of the objectives given in Equations (9), (10), and (11) as per Eq. (13). The CB radiation pattern is expected to have formed (with clearly identifiable sidelobes) by the 20th iteration. This deduction is based on typical outcomes observed in the CB process as per Fig. 5. The weighting values (g_x) have been carefully selected (adaptive) to yield the best possible outcome. In particular, the values ($g_1 = 0.5$), ($g_2 = 0.2$), and ($g_3 = 0.3$) have been used. This selection gives sidelobe minimization a slight edge over minimization of radiation in undesired directions: Minimization of radiation in undesired directions is already covered to some extent over the first 20 algorithm iterations.

$$\text{minimize} \qquad f(\mathbf{w}) = -g_1 \left|AF_{\phi_0,\theta_0}(\mathbf{w})\right|^2 + \left(g_2 \frac{\sum_u |AF_{\phi_u,\theta_u}(\mathbf{w})|^2}{C_u} + g_3 \frac{\sum_{SL} |AF_{\phi_{SL},\theta_{SL}}(\mathbf{w})|^2}{C_{SL}} \right) \tag{13}$$

A variant of the PSO algorithm has been utilized in optimizing (selecting the best possible node weights $\mathbf{w}$) Eqs. (12) and (13). *In cases featuring appreciable channel imperfections, node weights ought to be fine-tuned through a low-rate/short-time feedback mechanism.*

The performance of the proposed scheme has been validated from the perspective of traditional sidelobe suppression (peak side lobe suppression). This is in terms of:

- Observed average radiation power in the desired and undesired directions.
- Beamsteering accuracy.
- Side lobe levels.

Figure 5 illustrates typical radiation pattern plots obtained during an optimization run at the 1st, 20th, and final iterations, respectively. The beamsteering (sink) direction in this case is: 100 degrees azimuth, 55 degrees elevation. At the first iteration, the radiation pattern is poorly formed with the peak "placed" out of the desired direction. At the 20th iteration, the observed radiation pattern is well formed although with clearly identifiable and relatively high sidelobes. At the last iteration, an ideal radiation pattern (with radiation focused in the desired direction and suppressed in undesired directions) is observed.

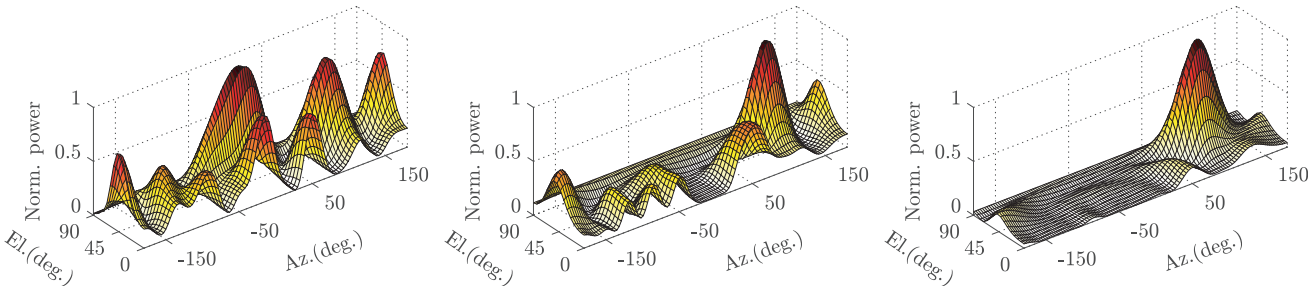

Figure 5. Typical radiation patterns: generated at the 1st, 20th and 60th iterations respectively.

4. SIMULATION FRAMEWORK

4.1. Simulation Platform

This research work has been modeled and analyzed through simulations in *Matlab* software. The *Matlab* platform provides a convenient programming and numeric computing platform suitable for beamforming schemes modelling, simulation, and analysis. The main mathematical tool utilized in this research (*the array factor*) can be easily modelled in *Matlab*. The graphical data presentation tools within *Matlab* are useful in beamforming results presentation, for instance, in presenting 3-dimension radiation pattern plots.

4.2. Simulation Variables

In this research work, a set of three aspects have been considered as per the list below.

(i) Comparative analysis of the proposed generalized sidelobe minimization scheme against peak sidelobe minimization and pure beamsteering.

(ii) Performance analysis of the proposed generalized sidelobe minimization scheme upon varying the number of collaborating nodes.

(iii) Performance analysis proposed generalized sidelobe minimization scheme upon varying the number of undesired radiation directions.

4.3. Results Analysis Tools

4.3.1. Normalized Array Factor

The basis of the CB schemes' performance analysis in this research is the Normalized Array Factor (NAF). The array factor gives a measure of the relative radiation strength in various directions (Section 2.1). The diverse CB schemes simulated in this research are bound to yield varying array factors. Array factor normalization gives room for fair performance comparison in diverse CB strategies. The NAF in the direction (ϕ, θ) is as per Eq. (14).

$$NAF_{\phi,\theta} = \frac{\mid AF_{\phi,\theta} \mid}{\max \mid AF_{\phi,\theta} \mid} \tag{14}$$

The Normalized Power Pattern (NPP) in the direction (ϕ, θ) is as per Eq. (15).

$$NPP_{\phi,\theta} = \left(\frac{\mid AF_{\phi,\theta} \mid}{\max \mid AF_{\phi,\theta} \mid} \right)^2 \tag{15}$$

The radiation pattern plots in this paper have been generated from the NPP as per Eq. (15). Sidelobe levels are easily picked from the NPP/radiation pattern plots.

4.3.2. Normalized Radiation Power in Desired and Undesired Directions

The normalized radiation power in the desired direction (sink direction) is extracted directly from the NPP given in Eq. (15). The normalized average radiation power in undesired directions is obtained by averaging the NPP (extraneous to the desired direction). This is done in a discrete manner over selected azimuth and elevation directions as per Eq. (16).

$$NARP_{\text{undesired directions}} = \frac{1}{TQ} \sum_{t=1}^{T} \sum_{q=1}^{Q} NPP_{\phi_q,\theta_t} \tag{16}$$

In Eq. (16), T is the total count of elevation directions, and Q is the total count of azimuth directions.

4.4. Statistical Data Analysis

In every optimization procedure in this research paper, 50 independent trials have been used. This fulfils the central limit theorem condition: sample sizes ≥ 30 [17]. This is vital towards application of the statistical tools used in this paper. The statistical tools used in this paper are:

- Analysis of Variance (ANOVA) test: tests whether two or more population means are statistically equivalent [18].
- Tukey-Kramer post-hoc analysis test: a test aimed at pinpointing the exact population means that bear statistically significant differences [19].

5. RESULTS AND DISCUSSION

5.1. Comparative Analysis of the Proposed Generalized Sidelobe Minimization Scheme, Highest Sidelobe Minimization Scheme, and "Pure" Beamsteering.

In this section, the performance of the proposed generalized sidelobe minimization scheme is compared against that of a scheme featuring peak sidelobe minimization only and that of pure beamsteering (without sidelobe minimization/suppression of undesired radiation). The used sink direction (beamsteering direction) is: 100 degrees azimuth, 55 degrees elevation.

5.1.1. Normalized Power Patterns

The normalized power pattern corresponding to CB with generalized suppression of radiation in undesired directions (*as per Equations (12) and (13)*) is as per Fig. 6(a). The normalized power pattern

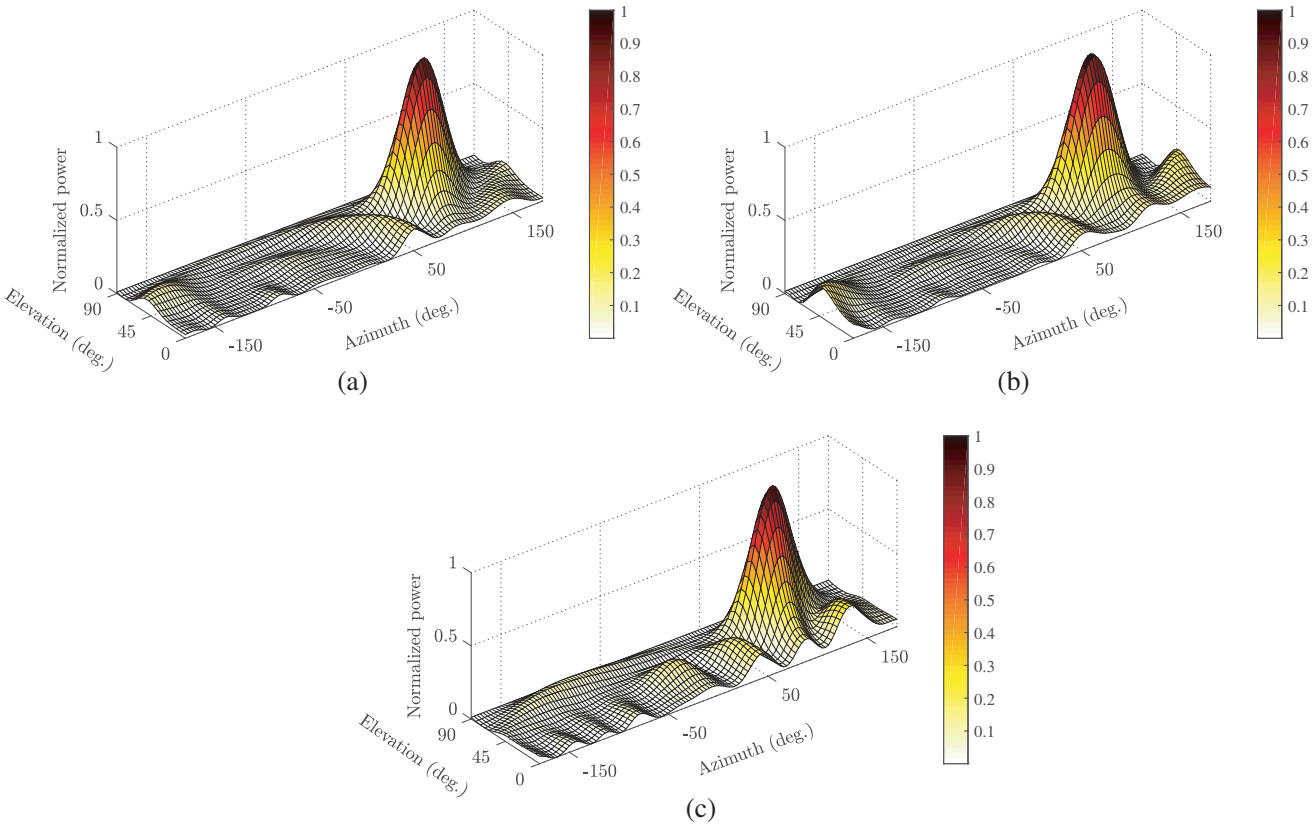

Figure 6. Average normalized power patterns. (a) With generalized suppression of radiation in undesired directions. (b) With peak sidelobe suppression only. (c) Beamsteering only.

corresponding to CB with peak sidelobe suppression only is as per Fig. 6(b). The normalized power pattern corresponding to a beamsteering only CB scheme is as per Fig. 6(c).

It can be qualitatively deduced (to some extent) that indeed the power patterns presented in Figs. 6(a) and 6(b) bear lower sidelobe levels/radiation in undesired directions in comparison to the power pattern presented in Fig. 6(c). A common observation in all the power patterns is that there is a clear-cut radiation peak oriented towards the intended radiation direction (100 deg. azimuth, 55 deg. elevation).

5.1.2. Normalized Power in the Desired Direction

The normalized power observed in the desired direction upon CB with/without undesired radiation suppression is as tabulated in Table 1. The tabulated data corresponds to the average outcome of 50 independent runs.

Table 1. Normalized power observed in the desired direction (averaged over 50 independent runs).

	Power in desired direction (normalized)	
	Average value	*SD*
Generalized radiation suppression	0.99683	0.00464
Peak sidelobe suppression	0.99544	0.00540
Beamsteering only	0.99759	0.00305

The "beamsteering only" scheme is associated with slightly higher radiation level in the desired direction than the other 2 schemes. By default, the "beamsteering only" criteria lay emphasis on maximization of radiation in the beamsteering direction only, unlike the other 2 schemes.

A statistical analysis of the quantified data is performed to establish if the differences observed in the normalized power data are statistically significant.

Analysis of variance results corresponding to *normalized power in the desired direction* is as tabulated in Table 2. The high P value (greater than 0.05) is indicative of absence of statistically significant differences in the means in the analyzed data-set.

Table 2. Analysis of variance: Normalized power in the desired direction.

Source	Sum of Squares	Degrees of Freedom	Mean Square	F-value	p-value
Between	0.000119	2	0.000060	2.981125	0.053812
Within	0.002939	147	0.000020		
Total	0.003058	149	0.000021		

5.1.3. Normalized Power in the Undesired Directions

The average normalized power observed in the undesired radiation directions upon CB with/without undesired radiation suppression is as tabulated in Table 3. The tabulated data corresponds to the

Table 3. Average normalized power observed in the undesired directions (averaged over 50 independent runs).

	Avg. power in undesired directions (normalized)	
	Average value	*SD*
Generalized radiation suppression	0.07998	0.00334
Peak sidelobe suppression	0.08599	0.00787
Beamsteering only	0.09647	0.01201

average outcome of 50 independent runs. The undesired radiation power has been evaluated at 1 degree resolution in both azimuth and elevation directions (outside of the half power region of the main beam).

A statistical analysis of the quantified data is performed to establish if the differences observed in the *average normalized power observed in the undesired directions* data are statistically significant.

Analysis of variance results corresponding to *normalized power in the desired direction* is as tabulated in Table 4. The low P value (less than 0.05) is indicative of the presence of statistically significant differences in the analyzed data-set.

Table 4. Analysis of variance: Average normalized power in the undesired directions.

Source	SS	df	MS	F	P
Between	0.006966	2	0.003483	48.093498	0.000000
Within	0.010646	147	0.000072		
Total	0.017613	149	0.000118		

The exact statistically significant differences in the data given in Table 3 are brought out in the Tukey-Kramer post-hoc analysis results presented in Table 5. In Table 5, "*General rad. supp.*" implies the proposed generalized undesired radiation suppression scheme, and "*PSL supp.*" implies the peak sidelobe suppression scheme. Power values corresponding to the 3 schemes under consideration are compared in a pairwise manner. In accordance to the Tukey-Kramer post-hoc analysis test, if the *Absolute Difference* value is greater than the *Critical Range*, the values under comparison are held as statistically different. It can be deduced that all means in Table 3 are statistically different. The implication is that the generalized radiation suppression scheme yields the lowest average radiation in undesired directions. The order of performance from best to worst is: *Generalized radiation suppression*, *Peak sidelobe suppression* and *Beamsteering only*.

Table 5. Tukey-Kramer comparison test: Normalized power in the undesired directions.

Comparison	Absolute Difference	Std. Error of Difference	Critical Range	Results
General rad. supp./PSL supp.	0.006017	0.00120353	0.0047	Means are different
General rad. supp./Beamsteering only	0.016493		0.0047	Means are different
PSL supp./Beamsteering only	0.010476		0.0047	Means are different

5.1.4. Beamsteering Accuracy

The absolute deviation of the direction of peak power from the desired direction upon CB with/without undesired radiation suppression is as tabulated in Table 6. The tabulated data corresponds to the average outcome of 50 independent runs.

Table 6. Absolute deviation (in degrees) of the direction of peak power from the desired direction.

Scheme	*Azimuth angle*	*Elevation angle*
Generalized radiation suppression	0.74	0.64
Peak sidelobe suppression	0.69	0.63
Beamsteering only	0.53	0.49

Analysis of variance results corresponding to *absolute deviation of the direction of peak power from the desired direction* is as tabulated in Tables 7 and 8. The high P values (greater than 0.05) are indicative of the absence of statistically significant differences in the analyzed data-sets.

Table 7. Analysis of variance: Azimuth angle deviation.

Source	SS	df	MS	F	P
Between	1.102500	1	1.102500	2.108753	0.149653
Within	51.236437	98	0.522821		
Total	52.338937	99	0.528676		

Table 8. Analysis of variance: Elevation angle deviation.

Source	SS	df	MS	F	P
Between	0.562500	1	0.562500	1.364068	0.245667
Within	40.412201	98	0.412369		
Total	40.974701	99	0.413886		

Tabulated in Table 9 are the percentages of direct "hits" from the perspective of perfect alignment between the direction of maximum power and the intended radiation direction.

Table 9. Percentage accuracy in beamsteering values.

Scheme	Azimuth	Elevation	Both Az. and El.
Generalized radiation suppression	56	58	44
Peak sidelobe suppression	55	53	42
Beamsteering only	64	60	48

Generally, the 3 schemes yield statistically equivalent beamsteering accuracy outcomes.

5.1.5. Sidelobe Levels

Achieved sidelobe levels are as per Table 10.

Table 10. Obtained average sidelobe levels.

SL	Generalized rad. suppression.	Peak SL suppression.	Beamsteering only.
1	0.1474	0.2050	0.2626
2	0.1472	0.2048	0.1849
3	0.1472	0.1499	0.1542
4	0.1162	0.0754	0.1021
5	0.0899	0.0743	0.0773
6	0.0837	0.0561	0.0562
7	0.0494	0.0531	0.0534
8	0.0476	0.0495	0.0501
9	0.0369	0.0410	0.0410
10	0.0186	0.0374	0.0395
Average	*0.0884*	*0.0947*	*0.1021*

SL reduction (%)	***13.43***	***7.32***

The Table lists the most prominent sidelobes observed in the average radiation pattern (obtained from 50 independent runs) in descending order. An average sidelobe reduction of 13.43% is observed in generalized radiation suppression and 7.32% in peak sidelobe suppression.

5.2. Performance Analysis upon Varying the Number of Collaborating Nodes

Herein, the generalized undesired radiation suppression scheme performance with variation in the number of collaborating nodes is comparatively analyzed. The utilized node arrangements are as per Fig. 7.

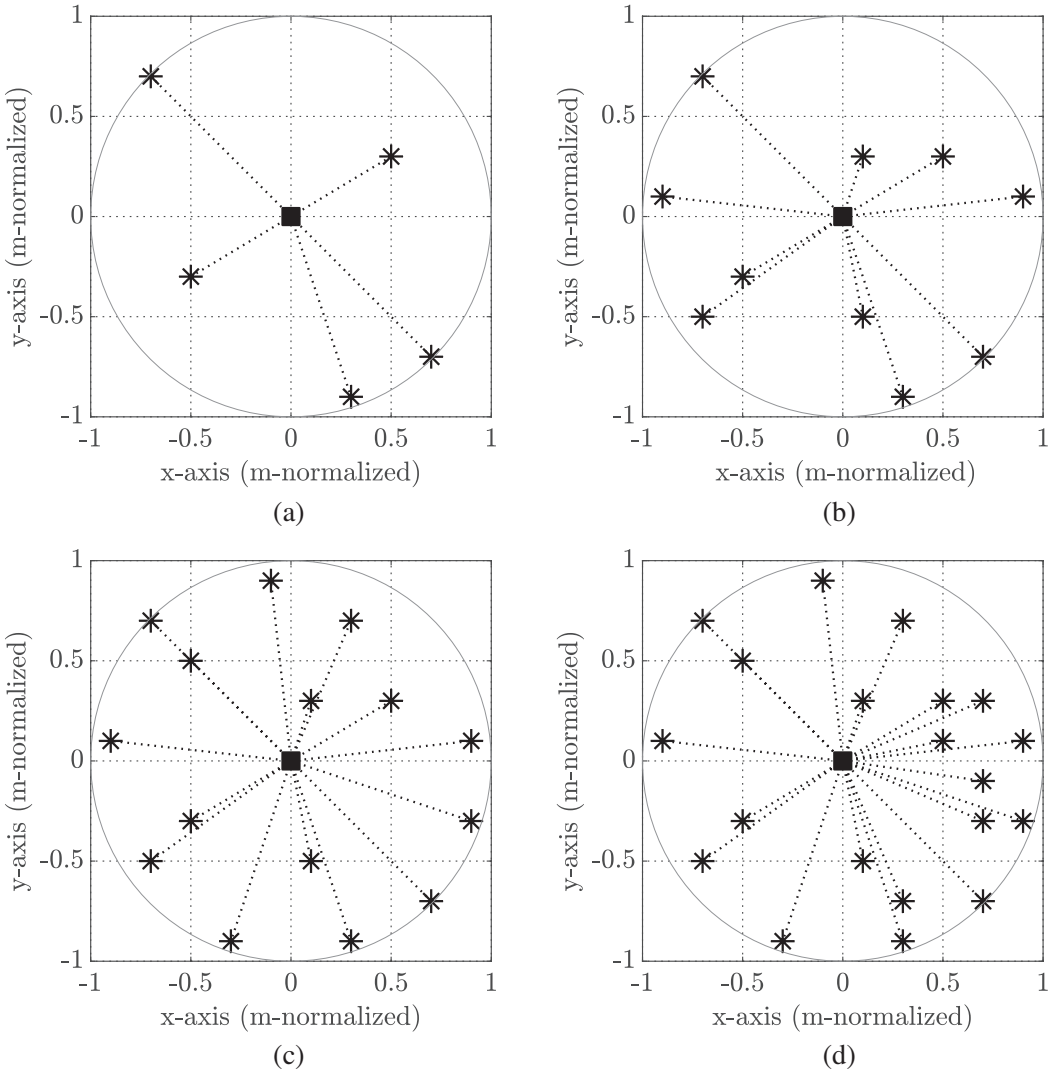

Figure 7. Cluster arrangements featuring node counts 5, 10, 15 and 20. (a) 5 node arrangement. (b) 10 node arrangement. (c) 15 node arrangement. (d) 20 node arrangement.

5.2.1. Normalized Power Patterns

Normalized power patterns in the form of mesh plots corresponding to CB (with generalized undesired radiation suppression) using 20, 15, 10, and 5 nodes are given in Figs. 8(a), 8(b), 8(c), and 8(d), respectively.

The presented power patterns are statistical averages corresponding to power patterns derived over 50 independent algorithm runs.

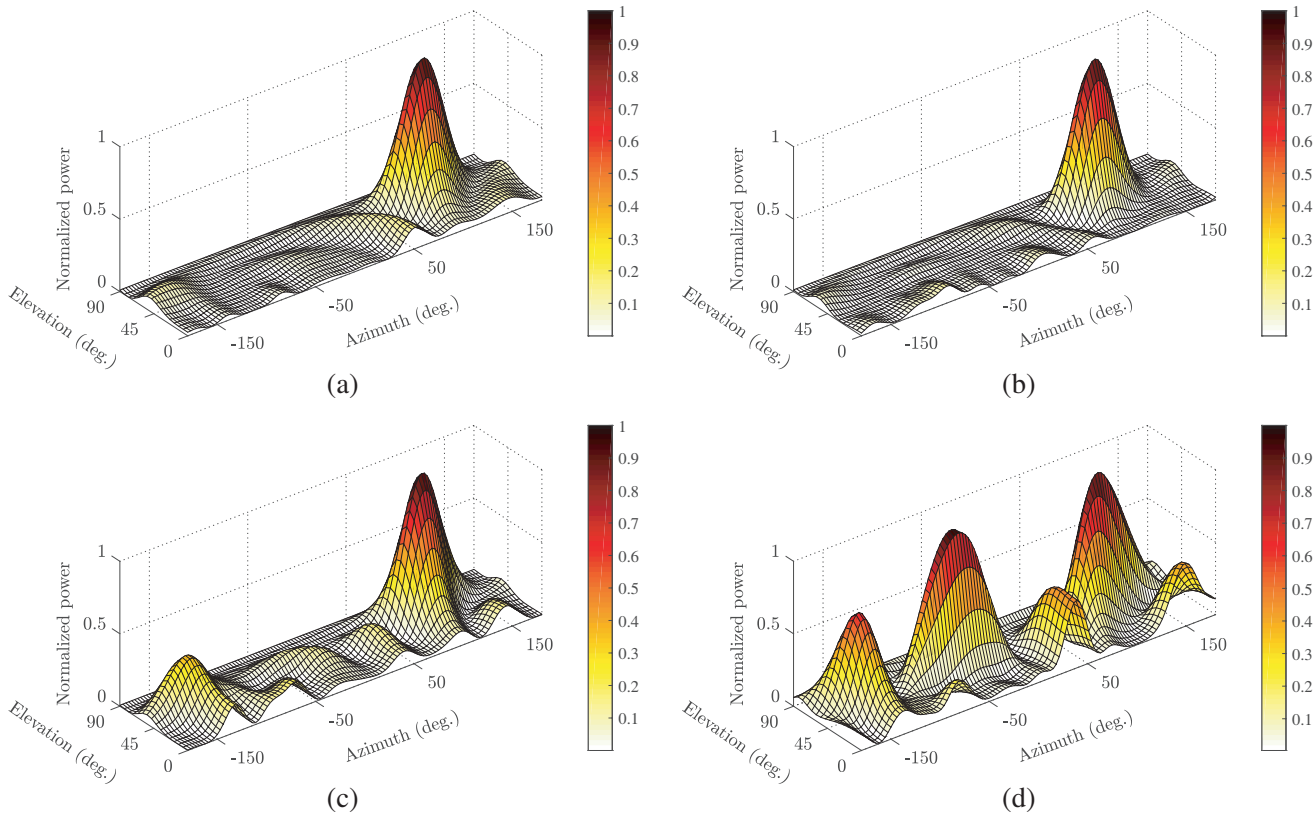

Figure 8. Average normalized power patterns. (a) 20 nodes. (b) 15 nodes. (c) 10 nodes. (d) 5 nodes.

It can be qualitatively deduced that indeed the power patterns presented in Figs. 8(a) and 8(b) (20 and 15 nodes) bear lower sidelobe levels than the power patterns presented in Figs. 8(c) and 8(d) (10 and 5 nodes). The power patterns in Figs. 8(a), 8(b), and 8(c) (20, 15, and 10 nodes) feature a clear-cut peak oriented towards the intended radiation direction (100 deg. azimuth, 55 deg. elevation).

5.2.2. Normalized Power Observed in the Desired and Undesired Directions

The normalized power observed in the desired and undesired directions using 20, 15, 10, and 5 nodes is as tabulated in Table 11. The tabulated data corresponds to the average outcome of 50 independent runs.

Table 11. Normalized power observed in the desired direction (averaged over 50 independent runs).

	Desired direction		Undesired directions	
	Average value	SD	Average value	SD
20 nodes	0.99683	0.00464	0.07998	0.00334
15 nodes	0.99148	0.00917	0.08262	0.00356
10 nodes	0.99221	0.00729	0.10515	0.00345
5 nodes	0.99086	0.00571	0.18017	0.00295

Analysis of variance test on the desired direction power data presented in Table 11 yields a P value 0.000069 (less than 0.05). This is indicative of the presence of statistically significant differences in the data-set. The exact statistically significant differences in the desired direction power data are brought

out in the Tukey-Kramer post-hoc analysis results presented in Table 12. It can be deduced that some of the means in Table 11 are statistically different.

Table 12. Tukey-Kramer comparison test: Normalized power in the desired direction.

Comparison	Absolute Difference	Std. Error of Difference	Critical Range	Results
20 nodes vs 15 nodes	0.005347	0.00097799	0.0038	Means are different
20 nodes vs 10 nodes	0.004627			Means are different
20 nodes vs 5 nodes	0.005972			Means are different
15 nodes vs 10 nodes	0.00072			Means are not different
15 nodes vs 5 nodes	0.000625			Means are not different
10 nodes vs 5 nodes	0.001345			Means are not different

The performance of the 20-node arrangement in terms of beamsteering (radiation power in the desired direction) is slightly superior to that of 5, 10, and 15 node arrangements (which bear statistically identical performance).

Analysis of variance test on the undesired directions power data presented in Table 11 yields a P value 1.5508E-213 (less than 0.05). This is indicative of the presence of statistically significant differences in the analyzed data-set. Going by Tukey-Kramer post-hoc analysis, all the undesired directions power data means in Table 12 are statistically different. The higher the number of collaborating nodes is, the better the undesired radiation performance is.

5.2.3. Graphical Analysis of the Data Given in Section 5.2.2.

Figures 9(a) and 9(b) portray graphical views of the results presented in Table 11. To allow for fair comparison, the graphs lie within equivalent normalized power scale (0.15). It is notable that the normalized power in the desired direction varies minimally with the count of collaborating nodes. The average normalized power in the undesired directions varies maximally in the low node count region and minimally in the high node count region. Deductively, the number of collaborating nodes does not bear a major impact on beamsteering capability in comparison to suppression of radiation in undesired directions.

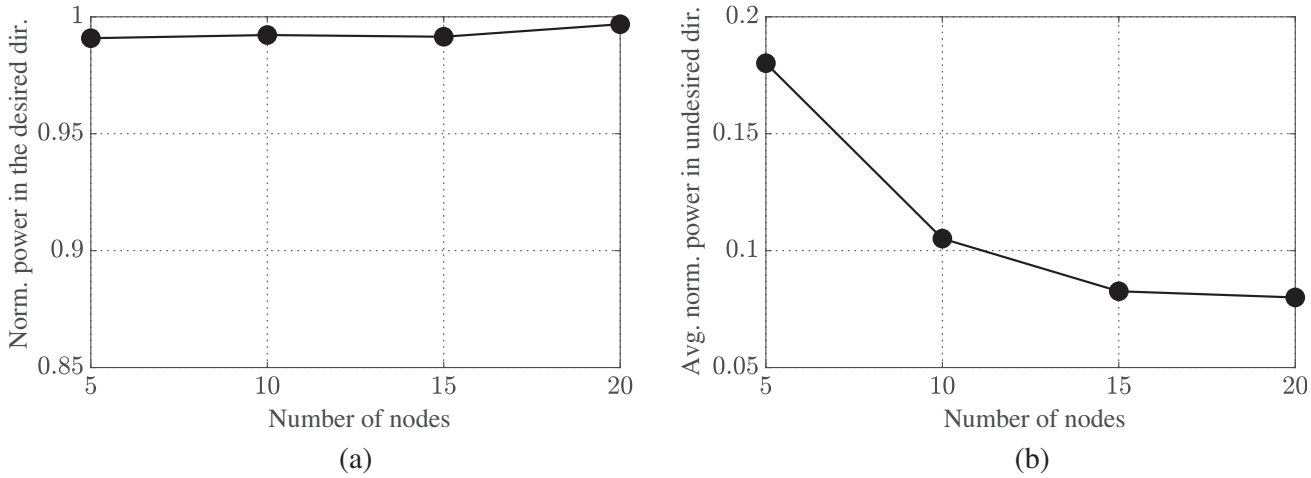

Figure 9. Average normalized power in the desired and undesired directions against count of nodes. (a) Average normalized power in the desired direction against count of nodes. (b) Average normalized power in the undesired directions against count of nodes.

5.3. Performance Analysis upon Varying the Number of Undesired Radiation Directions

Herein, the performance of the generalized undesired radiation suppression CB scheme is comparatively analyzed upon varying the number of selected undesired radiation directions. The utilized selections are as given earlier in Fig. 4.

The outcome of the analysis process is as per Fig. 10. The undesired radiation power has been evaluated at 1 degree resolution in both azimuth and elevation directions (outside of the half power region of the main beam). There is exponentially decaying improvement in undesired radiation suppression with increase in the number of selected undesired radiation directions. The improvement comes at the expense of a slight increase in computation complexity with increase in the number of selected undesired radiation directions.

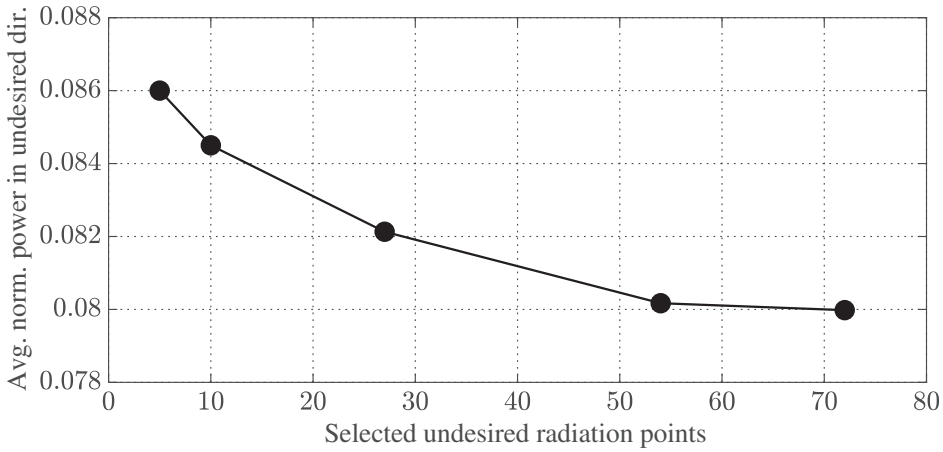

Figure 10. Average normalized power in the undesired directions against count of selected undesired radiation directions.

6. CONCLUSION

This paper has proposed a new approach towards suppression of undesired radiation upon CB in WSNs. The contributions brought forward in this paper include:

(i) Concurrent amplitude and phase optimization at collaborating nodes has been utilized towards achieving concurrent beamsteering and suppression of radiation in an elaborate set of undesired directions.

(ii) Generalized suppression of radiation in an expanded set of undesired directions has been proposed rather than suppression of the peak sidelobe only as per the current literature.

(iii) Investigations of items 1 and 2 above from the perspective of planar node arrangement with the sink at an elevated plane.

The proposed scheme outperforms the peak sidelobe suppression approach in terms of observed radiation in undesired directions and average sidelobe levels. It is noteworthy that the proposed radiation suppression scheme does not hamper beamsteering accuracy. It has also been established that increasing the number of collaborating nodes and/or the number of selected undesired radiation directions in the proposed CB scheme leads to exponentially decreasing undesired radiation performance improvement.

ACKNOWLEDGMENT

This work was supported by Institute of Basic Science, Technology and Innovation, Pan African University, Nairobi, Kenya.

REFERENCES

1. Jayaprakasam, S., S. K. A. Rahim, and C. Y. Leow, "Distributed and collaborative beamforming in wireless sensor networks: Classifications, trends, and research directions," *IEEE Communications Surveys & Tutorials*, Vol. 19, No. 4, 2092–2116, 2017.
2. Liang, S., T. Feng, G. Sun, J. Zhang, and H. Zhang, "Transmission power optimization for reducing sidelobe via bat-chicken swarm optimization in distributed collaborative beamforming," *2016 2nd IEEE International Conference on Computer and Communications (ICCC)*, 2164–2168, IEEE, 2016.
3. Liang, S., Z. Fang, G. Sun, Y. Liu, G. Qu, S. Jayaprakasam, and Y. Zhang, "A joint optimization approach for distributed collaborative beamforming in mobile wireless sensor networks," *Ad Hoc Networks*, Vol. 106, 102216, 2020.
4. Sun, G., X. Zhao, G. Shen, Y. Liu, A. Wang, S. Jayaprakasam, Y. Zhang, and V. C. Leung, "Improving performance of distributed collaborative beamforming in mobile wireless sensor networks: A multiobjective optimization method," *IEEE Internet of Things Journal*, Vol. 7, No. 8, 6787–6801, 2020.
5. Hasan, M. Z. and H. Al-Rizzo, "Beamforming optimization in internet of things applications using robust swarm algorithm in conjunction with connectable and collaborative sensors," *Sensors*, Vol. 20, No. 7, 2048, 2020.
6. Sun, G., X. Zhao, S. Liang, Y. Liu, Y. Zhang, and V. C. Leung, "A hybrid optimization approach for suppressing sidelobe level and reducing transmission power in collaborative beamforming," *2019 IEEE 90th Vehicular Technology Conference (VTC2019-Fall)*, 1–6, IEEE, 2019.
7. Liang, S., Z. Fang, G. Sun, Y. Liu, X. Zhao, G. Qu, Y. Zhang, and V. C. Leung, "Joint sidelobe suppression approach for collaborative beamforming in wireless sensor networks," *IEEE Access*, Vol. 7, 803–817, 2019.
8. Bao, X., H. Liang, and L. Han, "A novel node selection algorithm for collaborative beamforming in wireless sensor networks," *2018 IEEE International Conference on Internet of Things*, 345–349, IEEE, 2018.
9. Sun, G., Y. Liu, S. Liang, Z. Chen, A. Wang, Q. Ju, and Y. Zhang, "A sidelobe and energy optimization array node selection algorithm for collaborative beamforming in wireless sensor networks," *IEEE Access*, Vol. 6, 2515–2530, 2017.
10. Sun, G., Y. Liu, Z. Chen, A. Wang, Y. Zhang, D. Tian, and V. C. Leung, "Energy efficient collaborative beamforming for reducing sidelobe in wireless sensor networks," *IEEE Transactions on Mobile Computing*, 1–7, 2019.
11. Almagboul, M. A., F. Shu, Y. Qian, X. Zhou, J. Wang, and J. Hu, "Atom search optimization algorithm based hybrid antenna array receive beamforming to control sidelobe level and steering the null," *AEU — International Journal of Electronics and Communications*, Vol. 111, 152854, 2019.
12. Gravas, I. P., Z. D. Zaharis, T. V. Yioultsis, P. I. Lazaridis, and T. D. Xenos, "Adaptive beamforming with sidelobe suppression by placing extra radiation pattern nulls," *IEEE Transactions on Antennas and Propagation*, Vol. 67, No. 6, 3853–3862, 2019.
13. Zhao, W., J. Lin, S. Chan, and H.-H. So, "A division-free and variable-regularized lms-based generalized sidelobe canceller for adaptive beamforming and its efficient hardware realization," *IEEE Access*, Vol. 6, 64 470–64 485, 2018.
14. Zhou, M., X. Ma, P. Shen, and W. Sheng, "Weighted subspace-constrained adaptive beamforming for sidelobe control," *IEEE Communications Letters*, Vol. 23, No. 3, 458–461, 2019.
15. Sun, G., Y. Liu, H. Li, S. Liang, A. Wang, and B. Li, "An antenna array sidelobe level reduction approach through invasive weed optimization," *International Journal of Antennas and Propagation*, Vol. 2018, 2018.
16. Yang, F., G. Pei, L. Hu, L. Ding, and Y. Li, "Joint optimization of sinr and maximum sidelobe level for hybrid beamforming systems with sub-connected structure," *Digital Signal Processing*, Vol. 109, 102917, 2021.

17. Brooks, D., *The Sampling Distribution and Central Limit Theorem*, 1st Edition, Kindle, April 25, 2012.
18. Turner, J. R. and J. F. Thayer, *Introduction to Analysis of Variance: Design, Analyis and Interpretation*, 1st Edition, SAGE Publications, April 13, 2001.
19. Haynes, W., "Tukey's test," *Encyclopedia of Systems Biology*, Springer, New York, 2013.